The Search for M-M Dwarf Eclipsing Binary Systems

Jack B. Lubin

April 22, 2016

Contents

Abstract

Using data from the Kilodegree Extremely Little Telescope (KELT) project, we performed a survey of 2028 known M Dwarf stars in the KELT footprint for M-M Dwarf eclipsing binaries (EBs). After searching 2028 Mdwarf stars, we Follow up observation of our best target's eclipse events confirmed our hypothesis, and further Spectroscopic and Radial Velocity (RV) data allowed us to model the system. In this paper, we overview our survey and report the discovery and analysis of a new double-lined M-M eclipsing binary system, KS20C055996. This system is the second brightest M-M EB known (V$\sim$13.9) with M_1 = 0.47 $M_\odot$ and M_2 = 0.38 $M_\odot$, orbiting on a period of 1.11 days. KS20C055996 provides a unique opportunity to study Very Low Mass Stars (VLMS) and further compare observational results with current theoretical models of low mass stellar interiors.

1 Introduction

Mass and Radius, two of the most fundamental stellar parameters, are vitally important to understanding stellar evolution. Unfortunately, it can be difficult to measure these values to high precision. It is even more difficult to measure these values for Very Low Mass Stars (VLMS) with masses between 0.08 $M_\odot$, the lower limit of hydrogen fusion, and 0.30 $M_\odot$, the proposed upper limit of fully convective interiors for stars [Chabrier and Baraffe, 2000]. Also, there is a large discrepency between the observationally determined stellar properties and the one predicted by theoretical stellar models. These stars are important to our overall understanding of stellar astrophysics since, low mass stars (M Dwarf stars) make up the majority of all stars in our Galaxy [Lada, 2006].

Studying M Dwarfs, regardless of whether or not its masses fall within this classical definition, is important since our general understanding of these stars is quite limited. Also, it is important to study systems near the limits of this classical definition of VLMS, in turn helps to better constrain what those limits actually are and we can better understand the interior processes that occur in these stars. Isochrone fitting and stellar modelling of M Dwarfs often result in error bars of Mass and Radius up to 10+% [Terrien et al., 2015]. Such high error prompts the question, "Why do our models underestimate these parameters for VLMS, while providing more accurate values for medium and high mass stars? What is different about M Dwarfs?"

One suggested hypothesis concerns the nature of heat transfer within these stars. VLMS are thought to be fully convective down to their hydrogen-fusing cores. In contrast, more massive stars are known to be partially convective and partially radiative. For example, our Sun is known to comprise of both a Convective Zone and a Radiative Zone. In the former, hotter gas rises while cooler gas falls, creating convective heat cells within the envelope of the star while in the latter, photons carry

away energy as they random walk out of the star. The different interior structure of VLMS directly affects the magnetic fields surrounding the star, which in turn may inflate the radius of these stars [López-Morales and Ribas, 2005, Ribas, 2006], causing our models to under predict the true values.

In order to begin testing hypotheses on the causes of discrepancies between observation and model predictions, we need to precisely measure the mass and radius for additional M Dwarf stars. One method to directly measure radius is Interferometry. However, given the still young field of visible interferometry, the target star must be extremely bright, which is not a common feature of M Dwarf stars. Thus, it is nearly impossible to perform interferometry on M Dwarf stars. And even if it were viable, interferometry does not provide a mass measurement. Thus we are left to once again rely on stellar models to compute the mass via mass-radius or mass-luminosity relationships, which, as we have already stated, are subject to high error bars.

For these reasons, we turned to a different method of performing direct measurements of these basic stellar parameters: the classic two body problem of an Eclipsing Binary star system. Within a binary system, we can precisely measure the ratios of a host of stellar parameters between the two stars and then solve for the values of one, using tools like basic kinematic equations and Kepler's laws of motion. This method allows for accurate and, most importantly, model-independent mass, radius, and temperature.

All this stated, M-M Dwarf eclipsing binaries are seldom studied because they are difficult to find. In fact, only a handful of papers report discoveries of these systems, of which even fewer provide detailed analysis of the systems. The most well studied M-M EB, CM Draconis, is the brightest M-M Dwarf system at only V 12.87. The CM Draconis system has had its parameters constrained to within 1% [Morales et al., 2009] and has become a benchmark for all future work within the field. The system is made up of two nearly identical stars with Masses of M_1 = 0.2310 $M_\odot$ and M_2 = 0.2141 $M_\odot$ and Radii of R_1 = 0.2534 $R_\odot$ and R_2 = 0.2396 $R_\odot$. Many more systems like CM Draconis will be needed to provide enough data to test hypotheses concerning the model and observation discrepancies. There are only a few of these M-M Dwarf systems in the literature (see Figure 1).

In this paper, we overview the survey and report the results on a new double lined M-M Dwarf Eclipsing Binary, KS20C055996. Our system is the second brightest such system in the literature, only fainter than the famous CM Draconis system. This allows us to do extensive follow up observation. In this paper, we present a thorough analysis of this system in the effort to provide a new benchmark for future work and to add to the small list of M Dwarf stars for which we have model independent stellar parameters.

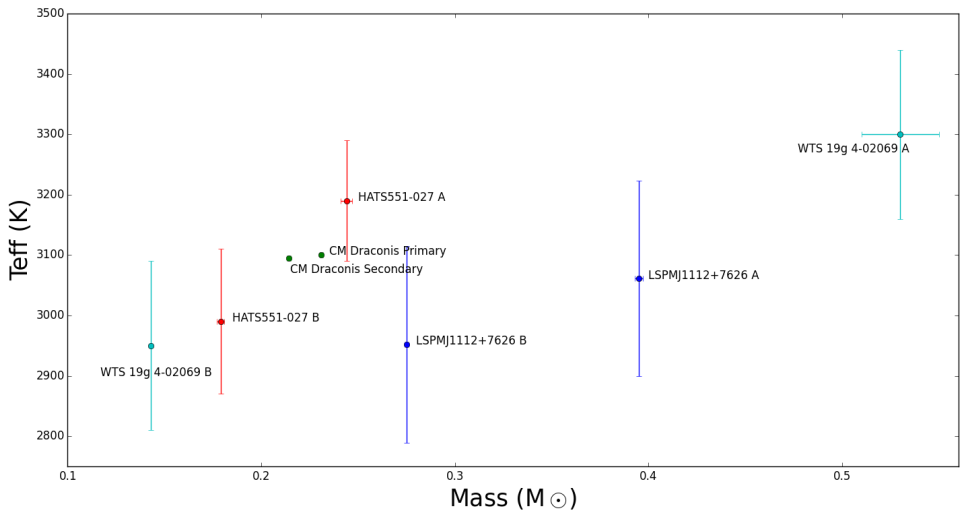

Figure 1: A recreation of Figure 8 from [Zhou et al., 2015] showing the mass and temperature of all known, bright (I $<$ 15) M-M Dwarf EBs.

2 The KELT Survey

For our survey, we used data from the Kilodegree Extremely Little Telescope (KELT) project. KELT is a unique set of twin telescopes owned and operated by Vanderbilt University, The Ohio State University, Lehigh University, and the South African Astronomical Observatory (SAAO). KELT-North [Pepper et al., 2007] is located at Winer Observatory near Sonoita, Arizona and KELT-South [Pepper et al., 2012] is located at the South African Astronomical Observatory in Sutherland, South Africa (See Figure 2).

The telescopes were designed for detecting transit events of Hot Jupiters around bright stars ($7 \leq V \leq 11$). Each telescope houses a 4096×4096 pixel CCD camera with a 42 millimeter aperture which produces very large field-of-view of $26^\circ \times 26^\circ$. The KELT surveys observe with a 10-20 minute cadence and all visible fields are observed each night, see Figure 3 for a celestial map of the KELT fields. The range in cadence depends on weather, the position of the Moon, and number of visible fields (10-20 minutes). Together, both telescopes observe over 70% of the entire sky.

The KELT Survey has been the basis for many exciting discoveries including 17 exoplanets ranging from Hot Jupiters to Brown Dwarfs. Ten of theses systems are in press of which 5 were found by KELT South. Additionally, KELT made an independent discovery of a WASP exoplanet. Beyond studying exoplanets, KELT has been used to study disk eclipses as well as a first light observation of M82 SN 2014J.

Finally, and perhaps most importantly, KELT works alongside a strong network

Figure 2: (Top) The KELT-South telescope located at the South African Astronomical Observatory (SAAO) in Sutherland, South Africa. (Bottom) The KELT-North located at Winer Observatory near Sonoita, Arizona.

of over 50 small college and experienced amateur astronomers. This worldwide network is capable of providing follow up photometric and spectroscopic observations to confirm exoplanet candidates and study a variety of variable stars.

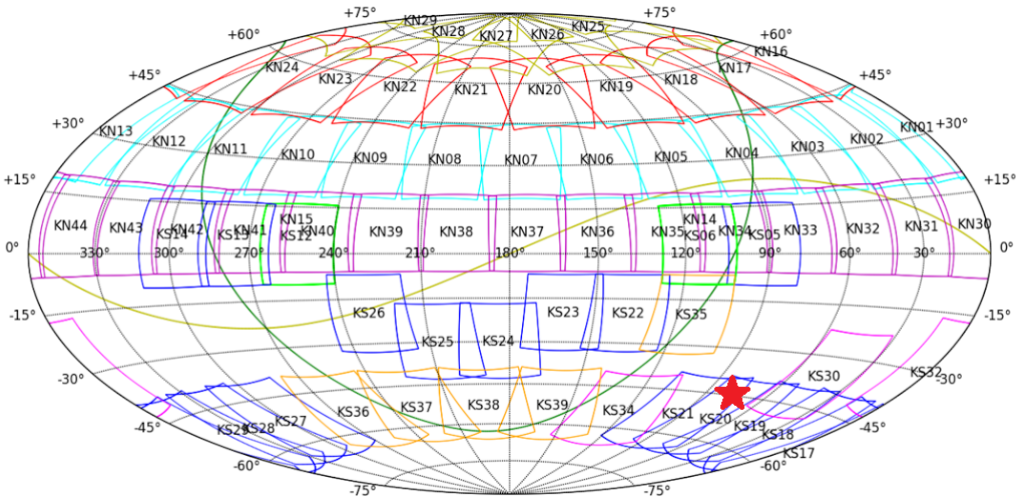

Figure 3: A celestial map showing the locations of the KELT fields. The different colors indicate when the field was added to the survey. The green line represents the galactic plane and the yellow line represents the ecliptic plane. Our system is located in KS20, indicated by a red star.

3 Methods and Procedure

3.1 Target List

To search for M-M EBs in KELT, we first built a list of all known M Dwarf stars, regardless of whether or not they were seen by KELT. This list was generated with the help of both Filtergraph Burger et al. [2013], a data visualization software developed by Vanderbilt University scientists, as well as the Transiting Exoplanet Survey Satellite (TESS) target list [Ricker et al., 2015, Pepper and Stassun, 2015].

$$RPM_J \leq -58 + 313.42X + 583.6X^2 + 473.18X^3 - 141.25X^4 \\ \Rightarrow where: X = J_{mag} - H_{mag} \tag{1}$$

The TESS catalog has over 3,000,000 stars of all spectral types in its target list. To narrow this down to just M Dwarf stars, we applied a series of cuts to larger set of stars. The first cut, concerning brightness, ruled out any stars of magnitude 13 or greater in the I band as this is near the faintness limit of KELT. Next, the temperature cut kept only stars with surface temperatures of less than 3840 K, the accepted maximum for spectral class M stars. The final two cuts concern proper motion; the first constraining true proper motion to less than 60 millearcseconds per year so as to ensure that our targets were relatively close to Earth, and finally an RPMJ cut (Reduced Proper Motion in the J Band). The equation used to make this cut line is designed to sift out M Giants from M Dwarf stars [Collier Cameron

et al., 2007], can be seen in Equation 1. Any star that falls above this polynomial is thought to be a giant star whereas those below the cut line are accepted as dwarf stars. In short, these cuts ensured us that: first, the targets were M stars; second, were bright enough to land in the KELT footprint; and lastly, were dwarf stars, not giants.

Our list of M Dwarfs within the TESS catalog came out to 77,228 stars, see Figure 4 for a visual breakdown of these stars using Filtergraph. We ran a cross matching code between these TESS targets and KELT's entire catalog to find the corresponding stars in the KELT catalog. This code used the Right Ascension and Declination coordinates for each target in our cut TESS list, and searched through the coordinates of every star in the KELT catalog, testing for matches. However, given errors in measurement or rounding, the coordinates for the same star in both catalogs may not be exactly the same. Therefore, we included a small search box around each coordinate in KELT to ensure that even small discrepancies in the coordinate lists did not result in good matches being thrown out.

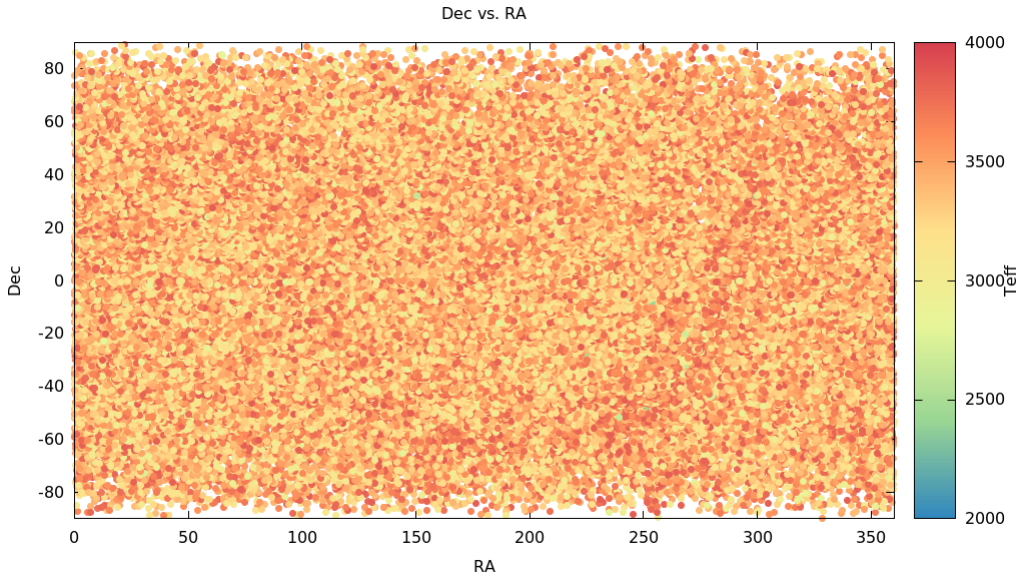

Figure 4: A visual display of the cuts we applied to the TESS target list. This plot was created using Filtergraph.

3.2 Searching for M-M Dwarf EBs

With our list of M Dwarfs within KELT finalized, we had approximately 7700 targets with corresponding KELT photometry. However, only 2028 of these targets had readily available detrended light curves. Since Mdwarfs are fainter than the optimal magnitude range of KELT, these stars have a larger photometric scatter

($\sim$10%) These detrended light curves were created using the Trend Filtering Algorithm (TFA) [Kovács et al., 2005] which used 150 nearby comparison stars of similar brightness to our target to look for common non-astrophysical trends. It then removed this baseline of trends from our target's photometry. From there, the first step in our search was to try to narrow down this list to only those that might be EBs. Using the Box Least Squares (BLS) periodicity algorithm [Kovács et al., 2002] in the VARTOOLS package [Hartman, 2012], a software developed at Princeton University for the sole purpose of finding transit and eclipse-like events in large data sets. BLS phase-folds the data set to a range of trial periods trying to fit a box-shaped transit at each step. BLS reports the best fit period for a possible eclipse or transit and the periodogram, which visually displays the confidence level of the best fit.

Using this best fit period, we plotted each star's lightcurve, phase-folded to the best fit period. In order to do this we wrote a program in Python which, when given the detrended raw data set of a star, as well as its BLS best fit period, it outputted the magnitude vs phase of the best fit BLS period (see Figures 5), and the BLS periodogram (see Figure 6). Table 1 shows the BLS statistics outputted from running the program on KS20C05596, including the original period of 0.55564452 days. Originally we believed this period might be half of the true period since BLS is not designed for finding two separate eclipse events, like an EB would show. Instead, we believed BLS was tricked into thinking that the two eclipses were actually one eclipse event, since both events are roughly similar in duration and depth given the similar sizes of these two stars. This would make the true period roughly double BLS's prediction and later follow up observations confirmed this hypothesis.

BLS Statistics	
Name	KS20C055996
Period 1 (days)	0.55564452
Tc (JD - 2450000)	5256.517167
SN	261.88714
SR	0.02291
SDE	22.78621
Depth	0.10367
Qtran (phase)	0.06667
delta chi2	-206.75865
Signal to pink noise	15.98969

Table 1: BLS statistics of our KS20C055996.

These graphs were then used as the basis for our visual analysis to deduce whether or not the period BLS suggested was significant. Usually, a visual analysis is not the ideal method for analysis; however, due to the reduced photometric precision, a visual analysis was the optimal way to select M-M EB candidates from

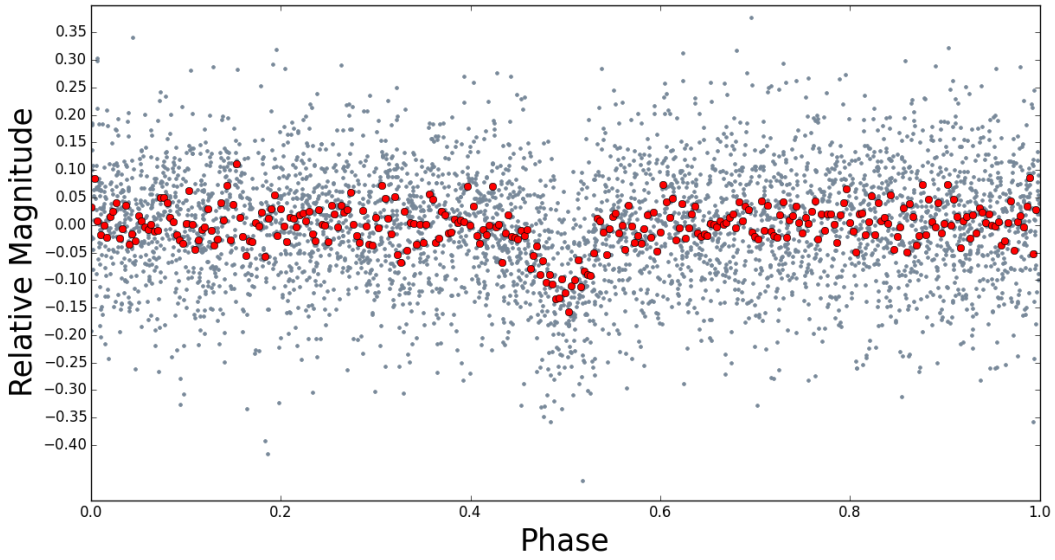

Figure 5: The original discovery plot of our system. Using BLS statistics, we phase folded the data to a period of 0.55564452 days. We later determined this to be roughly one half the true period.

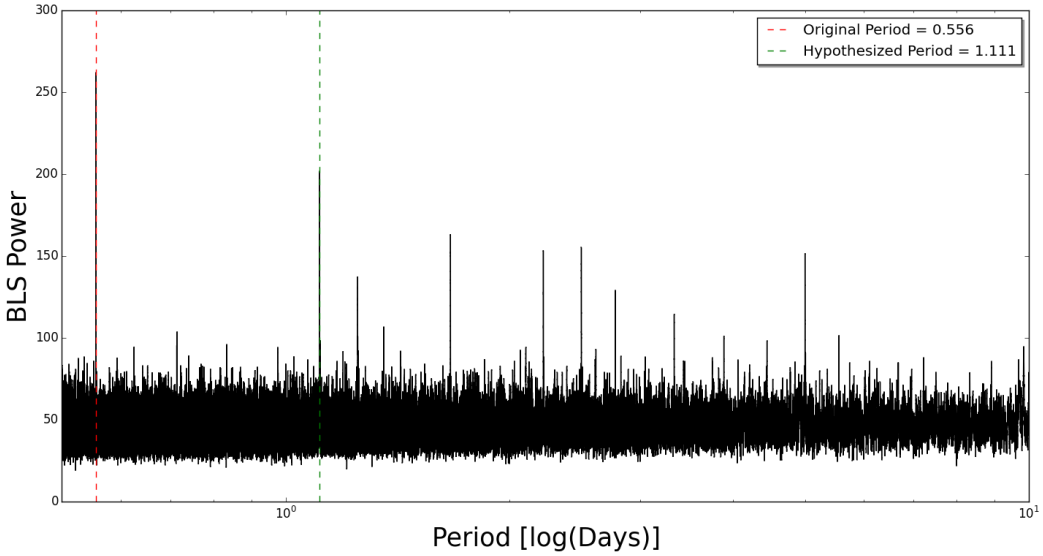

Figure 6: The periodogram outputted by the BLS program. It shows the strength of confidence of the best fit period, in this case 0.55564452 days where we have a tall and distinct peak, indicating high confidence.

the 2028 KELT M-stars in our set. There were a few things in particular that we looked for in visually inspecting the graphs. First, we looked for any obvious clear, coherent dimming event. If there was a dip, we inspected how deep it was, how long it lasted relative to the phase, and how wide the dip was. Then we checked to see if the event repeated itself within the phase time. If the dip was deep and wide enough, we knew it could not be a planetary event and so we assigned the star as an EB candidate. While looking for these characteristics, we saw many other features in the plots that were of note, including shallow, box like dips, and also sine curves. These we attributed to potential planetary events and to rotational curves respectively.

4 Observations

Out of the 2028 light curves we analyzed, we periodically sorted light curves by their level of interest to our work, giving each one of these marked targets more attention and scrutiny than the average. At the completion of this process, three top candidates were found. These three targets were KS23C095207, KS19C074212, and KS20C05596.

4.1 False Positives

One concern we had with these targets derived from the nature of the KELT survey. Given the relatively large pixel size of the telescopes (23"/pixel), it was possible that the events we believed we were seeing could have been from another object blended with our target. In order to confirm that the event we were seeing was indeed coming from the target of interest, we looked at the difference images during the time of the BLS determined eclipse. In these plots, Figures 5, 6, and 8, the target is located inside the green circle, and white pixels are the location of the dimming during the time of proposed eclipse.

4.1.1 KS19C074212

Figure 7 shows the plot for KS19C074212. Looking near the green target, it is clear that the pixels surrounding it to the Northwest are white, indicating that region became dimmer. Meanwhile, off to the Southwest, there is a large black spot which indicates that that region got brighter. Because this dimmer region is outside the target circle, we came to the conclusion that the signal we interpreted as a possible eclipse was actually not coming from our target and therefore this was not an EB. Whatever event we were seeing was a blend of some other nearby object with the target star. Therefore, we ruled this target to be a false positive and eliminated it from any future observation.

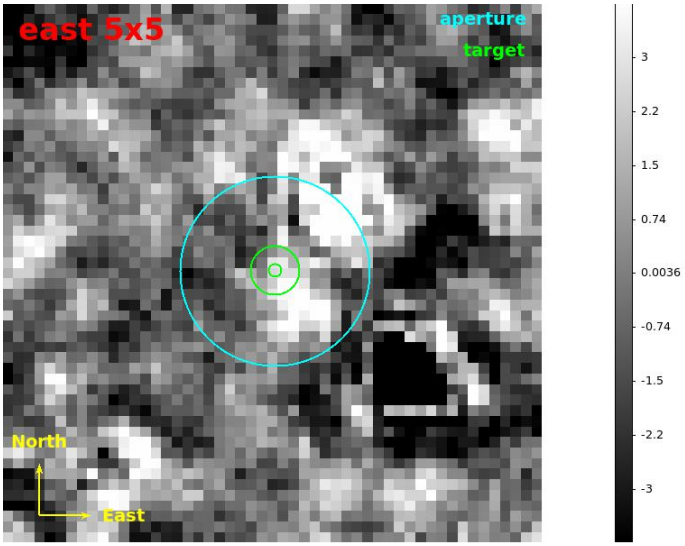

Figure 7: Time of eclipse image for KS19C074212, ruled a false positive due to blending from the Northwest.

4.1.2 KS23C095207

Figure 8 shows the plot for KS23C095207. This image clearly shows two objects to the North that are getting dimmer during the time of the proposed eclipse, as evidenced by the white pixels. Both objects are outside the green circle of our target and therefore we believed the signal we had recorded was a blend from these two nearby objects. This target was ruled out from our search.

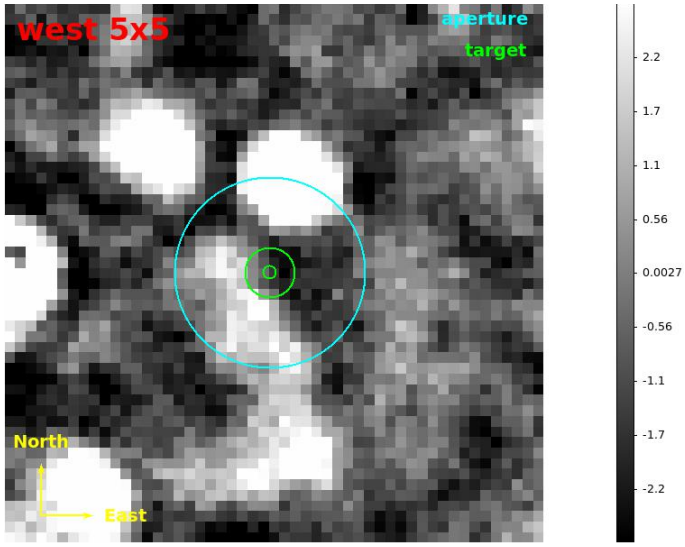

Figure 8: Time of eclipse image for KS23C095207, ruled a false positive due to blending from the North.

Parameter Names	Description	KS20C055996 Value 2MASS J04162165-6200463 UCAC4 140-003916 WISE J041621.52-620047.1	Source	Reference(s)
α_{J2000}	Right Ascension (RA)	04:16:21.652	UCAC4	Zacharias et al. [2012, 2013]
δ_{J2000}	Declination (Dec)	-62:00:46.44	UCAC4	Zacharias et al. [2012, 2013]
B	UCAC4 magnitude	15.368±0.03	UCAC4	Zacharias et al. [2012, 2013]
V	UCAC4 magnitude	13.877±0.01	UCAC4	Zacharias et al. [2012, 2013]
J	2MASS magnitude	10.234 ± 0.026	2MASS	Cutri et al. [2003], Skrutskie et al. [2006]
H	2MASS magnitude	9.589 ± 0.023	2MASS	Cutri et al. [2003], Skrutskie et al. [2006]
K	2MASS magnitude	8.758 ± 0.0189	2MASS	Cutri et al. [2003], Skrutskie et al. [2006]
WISE1	WISE passband	9.239 ± 0.023	WISE	Cutri et al. [2012]
WISE2	WISE passband	9.107 ± 0.02	WISE	Cutri et al. [2012]
WISE3	WISE passband	8.971 ± 0.02	WISE	Cutri et al. [2012]
WISE4	WISE passband	9.239 ± 0.023	WISE	Cutri et al. [2012]
μ_α	Proper Motion in RA (mas yr^{-1})	-73.8 ± 1.5	UCAC4	Zacharias et al. [2012, 2013]
μ_δ	Proper Motion in DEC (mas yr^{-1})	-70.9 ± 1.5	UCAC4	Zacharias et al. [2012, 2013]

Table 2: Stellar Properties of KS20C055996 obtained from the literature.

4.2 KS20C055996

Through the 2028 light curves, one in particular stood out, KS20C055996. Its light curve, phase folded to its period of 1.1112884 days, can be seen in Figure 9. The primary eclipse at phase of 0.25 is an 18% reduction in magnitude and its dip pattern is a V shape as opposed to a box shape, indicating an eclipse rather than the transit of a smaller object in front of the disk of the companion star. The secondary eclipse occurs at the 0.75 phase mark and is smaller in depth, only 13%, but still deeper than any planetary transit event would show. Furthermore, we searched through the literature to find all available data on this target, which can be seen in Table 2.

Just as with the other two final candidates, we needed to be sure that the signal was truly coming from our target. Figure 10 shows the in-eclipse plot for KS20C055996. This image very clearly shows white pixels directly inside the green target circle, indicating that our dimming signal was indeed coming from the target.

Having ruled out the possibility of this being a clear blend, we continued to confirm that this object was what we thought it was, namely an M-M Dwarf EB. Using the KELT follow up team, we secured secondary photometric observations to independently confirm the eclipse events, as well as spectroscopic and RV measurements.

4.2.1 Photometric Follow Up

Hazelwood Observatory

Operated by Chris Stockdale, the Hazelwood Observatory is located in Victoria Australia. This backyard observatory hosts a 0.32 m Planewave CDK telescope using a SBIG ST8XME 1.5K $\times$ 1K CCD. This setup gives a $18' \times 12'$ field of view

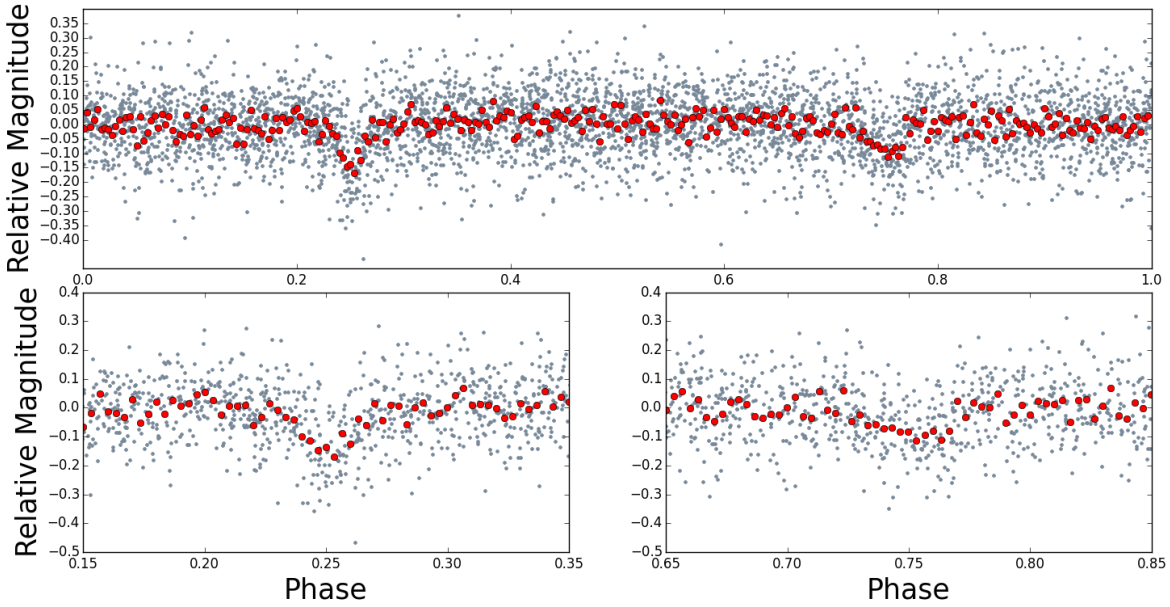

Figure 9: Four seasons of KS20C055996 phase folded to our determined period of 1.1112884 days.

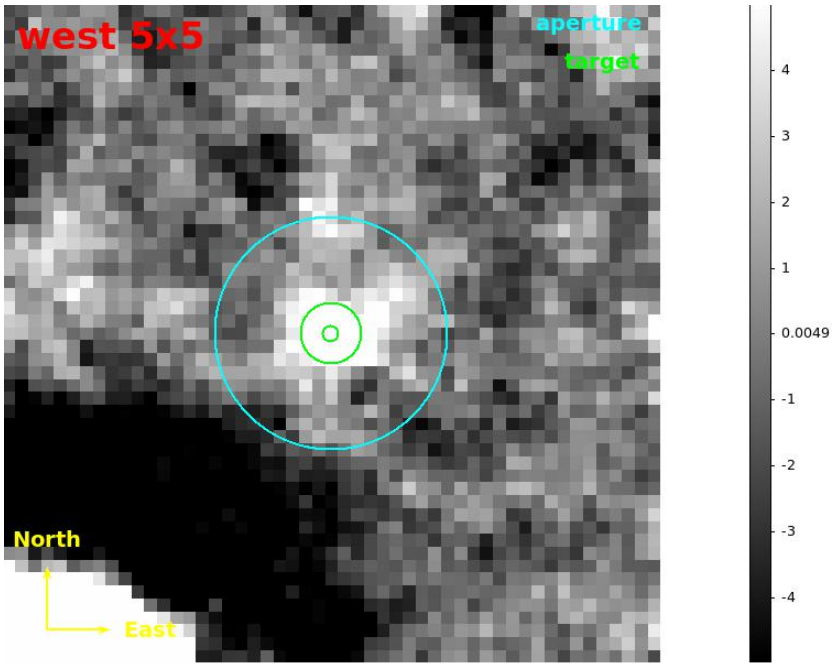

Figure 10: Time of eclipse image for KS20C055996, our best target. Our signal was confirmed as coming from our target of interest.

with 0.73″ per pixel. Using the 0.32m telescope, an observation of the primary eclipse of KS20C055996 was observed on UT 2015 December 28th in the R band and on UT 2015 October 17th in the B band. An observation of the secondary eclipse was observed on UT 2015 October 14th in the V band (see Table 3).

Myer's Observatory

T50 is a PlaneWave Instruments CDK17 17 inch (0.43 m) f/6.8 Corrected Dall-Kirkham Astrograph telescope. It is owned and remotely operated from California by Gordon Myers. The telescope is located at Siding Spring, Australia; on site support is provided by iTelescope[1]. The camera is a Finger Lakes Instruments (FLI) ProLine Series PL4710 - E2V 47-10-1-353 Back Illuminated Broadband Monochrome CCD with the Basic Mid-band coating. iTelescope's customized version of ACP software is used to script, schedule, and operate the telescope. The scope has U, B, V, R, I, Clear and Luminance filters. Three full transits of KS20C055996 were observed – two with an I filter (with 120 second exposures) on UT 2015 October 11 and (30 second exposures) on UT 2016 February 14 and one with a B filter (with 300 second exposures) on UT 2016 January 11 (see Table 3).

SkyNET

Using the Skynet network of worldwide telescopes [Reichart et al., 2005][2], we observed a secondary eclipse of KS20C055996 on UT 2015 September 30 in the V band. Specifically, we used the 0.4 m Prompt5 telescope from the PROMPT (Panchromatic Robotic Optical Monitoring and Polarimetry Telescope) subset of the Skynet network located at CTIO. The Prompt5 telescope uses an Alta U47s Apogee camera. This set up corresponds to a 10'$\times$10'field of view with a 0.59″ pixel^{-1} pixel scale (see Table 3).

Figure 11 shows the photometry from all these follow up observations, plotted in phase just like the discovery plot. It is color coded for the different observatories. All four of the primary eclipse follow up observations are consistent with our original observation, and similarly so for the secondary eclipse. In this display, each of the observations of the primary eclipse are offset from one another by 0.15 magnitudes while the secondary eclipse is offset by 0.30 magnitudes, just so they can be easily seen on the plot. The MyersB observation (black dots), experience some cloud cover towards the end of the eclipse and thus some of the data points are outliers.

4.2.2 Spectroscopic Follow Up

A series of spectroscopic follow-up observations were performed to characterise the atmospheric properties and radial velocity variations of KS20C055996. These observations were performed using the Wide Field Spectrograph (WiFeS) on the

[1] www.iTelescope.net

[2] https://skynet.unc.edu/

Table 3: Photometric follow-up observations and the detrending parameters found by AIJ for the global fit.

Observatory	Date (UT)	Filter	FOV	Pixel Scale	Exposure (s)
Skynet Prompt5	UT 2015 September 30	V	$10' \times 10'$	$0.59''$	300
Myers	UT 2015 October 14	I	$15.5' \times 15.5'$	$0.92''$	120
Hazelwood	UT 2015 October 14	V	$18' \times 12'$	$0.73''$	300
Hazelwood	UT 2015 October 17	B	$18' \times 12'$	$0.73''$	300
Hazelwood	UT 2015 December 28	R	$18' \times 12'$	$0.73''$	300
Myers	UT 2016 January 11	B	$15.5' \times 15.5'$	$0.92''$	300
Myers	UT 2016 February 14	I	$15.5' \times 15.5'$	$0.92''$	30

NOTES
All the follow-up photometry presented in this paper is available in machine-readable form in the online journal.

ANU 2.3m telescope, at Siding Spring Observatory, Australia. WiFeS is an image slicer integral field spectrograph, with a spatial resolution of 1"per spatial pixel in the $2\times$ bin mode. Our observing strategy, reduction, and analyses techniques are detailed in full in Zhou et al. [2015], and discussed below.

Spectroscopic classification of the binary was obtained with a $\lambda/\Delta\lambda \equiv R = 3000$ spectrum, converting the wavelength range of 3500-9000Å. The spectrum was flux calibrated as per Bessell [1999], using spectrophotometric standard stars calibrated in Hamuy et al. [1992] and Bessell [1999]. The flux calibrated low resolution spectrum of KS20C055996, is plotted in Figure 12. We match the spectrum to the synthetic spectral templates from the BT-Settl atmosphere models [Boyajian et al., 2012], adopting the Asplund et al. [2009] abundances. The surface gravity is fixed to $\log g = 5$, as this is the expected gravity for M-dwarfs [e.g. Baraffe et al., 1998, Dotter et al., 2008]. We find a best fit effective temperature for KS20C055996, of $T_{\rm eff}$= 3340$\pm$85 K.

The WiFeS spectra of GJ 191 (3570$\pm$156K) [Ségransan et al., 2003] and GJ 699 3224$\pm$10 K [Allard et al., 2012] are plotted for comparison. Metallicity is estimated by measuring the ζTiO/CaH index [Reid et al., 1995] using the calibration from Lépine et al. [2013], finding a metallicity of [M/H]=-0.2$\pm$0.2.

4.2.3 Radial Velocity Follow Up

Radial velocities are measured from WiFeS multi-epoch medium resolution observations, at $R = 7000$, over the wavelength range of $5200 - 7000\,\mathring{A}$. A total of six observations were obtained over 20150930 to 20151005, see Figure 13. To measure the radial velocities of both stellar components in the spectra. We cross correlate the spectra against nine M-dwarf standards observed by WiFeS, ranging over the spectral classes of M1.5 to M4.0. The cross correlation functions (CCF) from all the exposures are fitted simultaneously with double Gaussians, where each CCF has

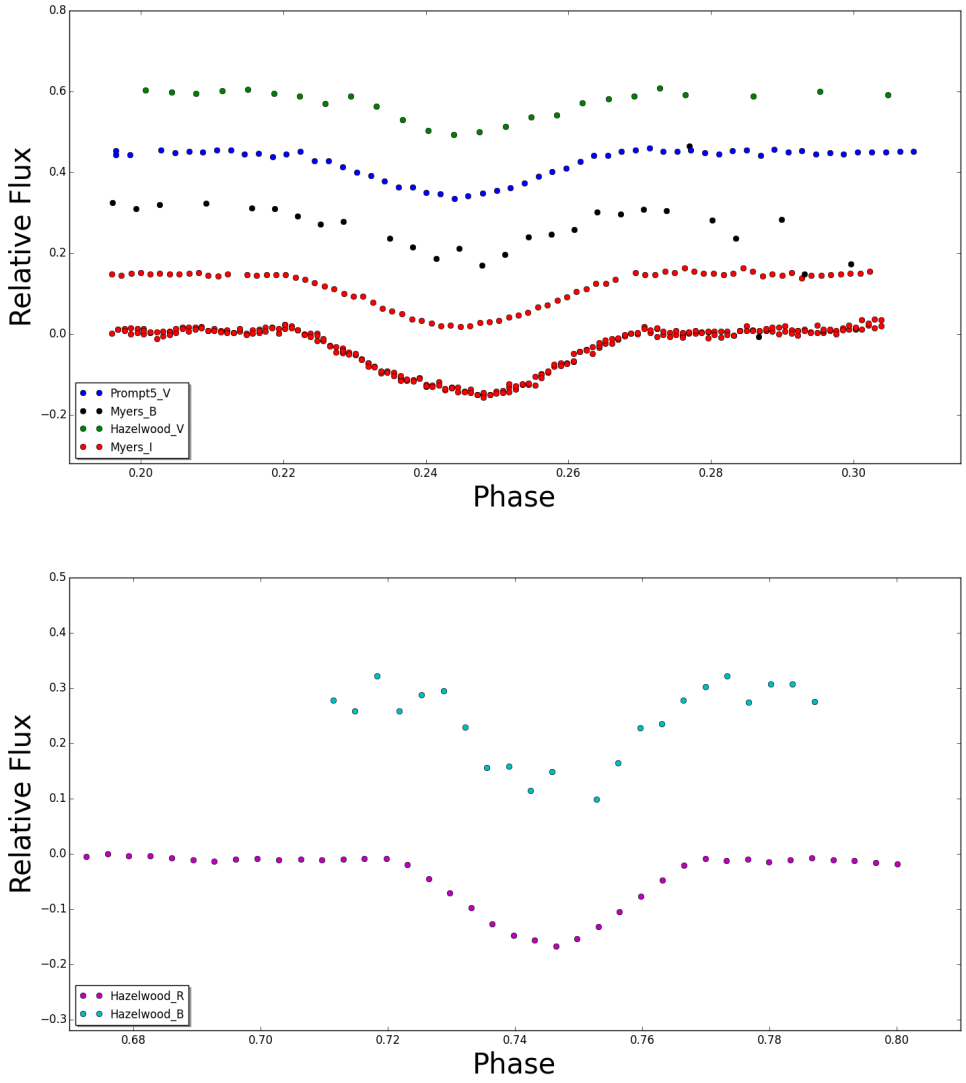

Figure 11: A zoom in on each eclipse from the photometric follow up observations. Observatories are color coded.

free parameters of velocity centroids v_1, v_2, while the parameters light ratio L_2/L_1, and CCF widths are shared amongst all exposures. The best fit parameters and per-point uncertainties are estimated from an MCMC analysis, using the *emcee* implementation of an affine invarianet ensemble sampler [Foreman-Mackey et al., 2013]. We apply this same velocity fitting procedure to the sets of CCFs derived from each M-dwarf template to understand the template spectral type dependence of the radial velocity measurements. The scatter in the velocity measured for each point for the set of models is then added in quadrature to the mean velocity uncertainty from the MCMC analysis. We also measure a light ratio of $L_2/L_1 = 0.43 \pm 0.03$ from the

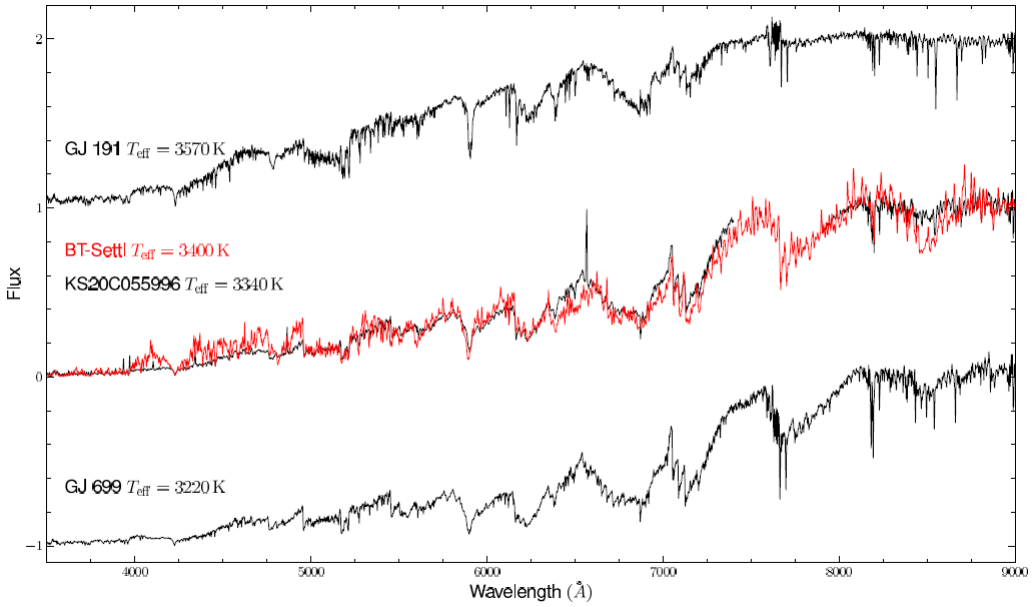

Figure 12: Spectral Analysis

relative heights of the CCFs, this is subsequently used to constrain the global fitting.

As with many other short period M-M binaries, the Balmer and Calcium H & K lines are found in emission due to stellar activity. López-Morales [2007] found a correlation between the activity index and the relative model-observation radius discrepancy of M-dwarf binaries. We use the WiFeS $R = 7000$ spectrum to estimate the Hα flux in each stellar component of KS20C055996. We measure Hα luminosities of $\log L_{H\alpha}/L_{Bol} = -3.7 \pm 0.1$ and -4.0 ± 0.1 for the two components of KS20C055996, derived from the two WiFeS exposures take on 20151002 and 20151005 at phase quadratures.

5 Results and Discussion

5.1 Model

In order to obtain a first estimate of the ”average” temperature of the stars, we first fit the combined-light spectral energy distribution (SED) of the system using catalog photometry from GALEX, APASS, 2MASS, and WISE spanning a wavelength range of 0.15–20 um (See Table 2). The fitted SED model is a NextGen stellar atmosphere model with free parameters of Teff, Av, and distance (we adopted a main-sequence surface gravity of 5.0 and solar metallicity). This initial fit yielded a best-fit Teff = 3350 +/- 50 K and Av = 0.03 +/- 0.03 mag, see Figure 14.

Next, we used the Phoebe eclipsing binary modeling program (based on the Wilson-Devinney EB modeling code) to fit the radial velocities and the multi-band

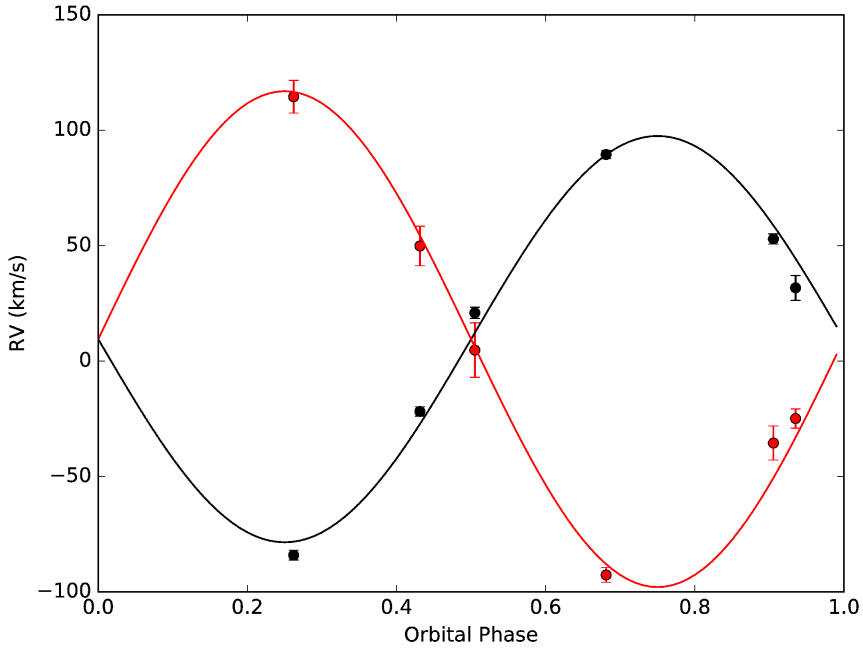

Figure 13: Radial velocity measurement of both M_1 (Black) and M_2 (Red) with a corresponding circular orbital fit.

light curve data. We fit the RVs for the sum of the stellar masses (modulo sin3i), the orbital semi-major axis (modulo sini), the mass ratio (q), and the center-of-mass velocity (Vgamma). We fit the light curves for the sum of the stellar radii (R1 + R2), the ratio of effective temperatures (T2/T1), and the orbital inclination angle (i). The latter together with the RV fitted parameters then yields the individual stellar masses, M1 and M2 (See Figure 15).

To establish the individual stellar temperatures and radii, we next used the spectroscopic flux ratio from the WIFES spectra of F2/F1 = 0.43 over the wavelength range 0.52–0.70 um. We re-fit the combined-light SED as above, but this time using the sum of two stellar atmospheres whose flux-weighted average temperature is 3350 K and whose temperature ratio is as given from the light curve modeling above. The only free paramater then is the radius ratio required to produce a flux ratio in the 0.52–0.70 um range of 0.43. This results in individual temperatures of T1 = 3395 K and T2 = 3245 K, and a radius ratio of R2/R1 = 0.814. Together with the radius sum from the light curve model above, we obtain the individual radii.

5.2 Conclusions

With good fits from the model, we are confident in our expected parameters which show Masses of $M_1 = 0.46\ M_\odot$ and $M_2 = 0.39\ M_\odot$ and Radii of $R_1 = 0.51\ R_\odot$ and

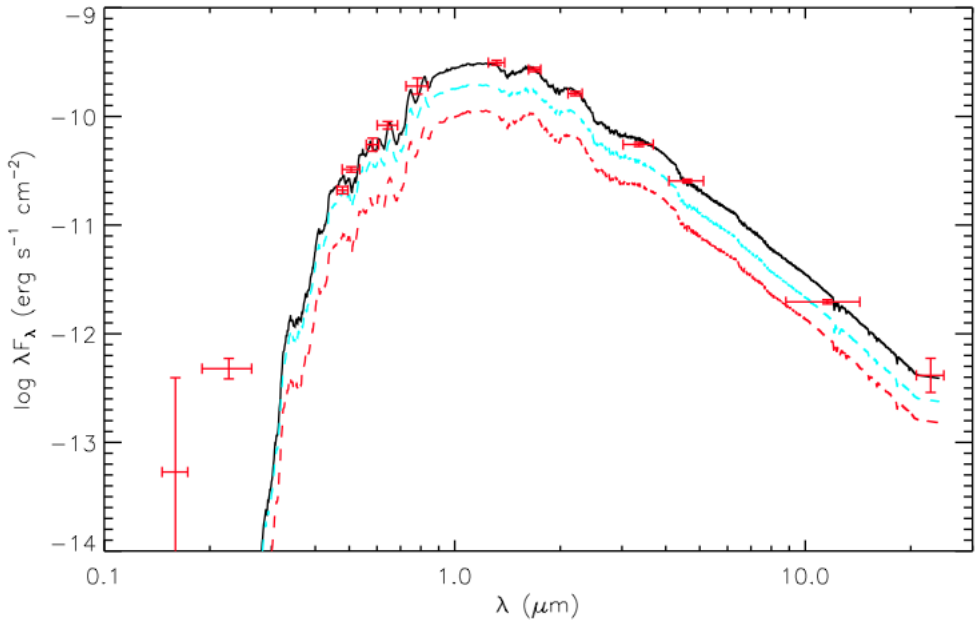

Figure 14: A Spectral Energy Density from the model. The red points with error bars are observational data of the combined light of both objects. The red and blue lines are the best fit from the model for the two individual stars. The black line is the sum of the red and blue lines to create a best fit from the model for the combined light.

$R_2 = 0.42\ R_\odot$. Unfortunately, an error analysis is still pending and is not complete at this time of this these defense. With these parameters in mind, we return to Figure 1 from earlier which shows all the known bright M-M Dwarf EBs, only now we place our system on the plot (see Figure 17).

Our system is comprised of two very alike stars in their masses, temperatures, and radii. While their masses are on the upper end of the classical definition of VLMS, we understand that limit to be a suggestion which needs further data to cement into place. We believe our system provides a new opportunity to help set that upper limit and for future study of the interiors of low mass stars.

While we are very excited about this system, there is still plenty of work to be done in the future. As mentioned before, this system was found in a subset of 2000 known M Dwarf stars in the KELT Survey which totals about 7700 M Dwarf; however, there are still another 5700 stars yet to be analyzed. We believe there could be another 5 potential M-M Dwarf EBs in this unexplored data set. This number is based off of some rough calculations: 20% of all M dwarf stars are in binaries, 10% of binary systems have periods less than 10 days, and 6% of systems are oriented correctly for a transit event with respect to Earth. Multiplying these together gives a detection rate of 0.1%.

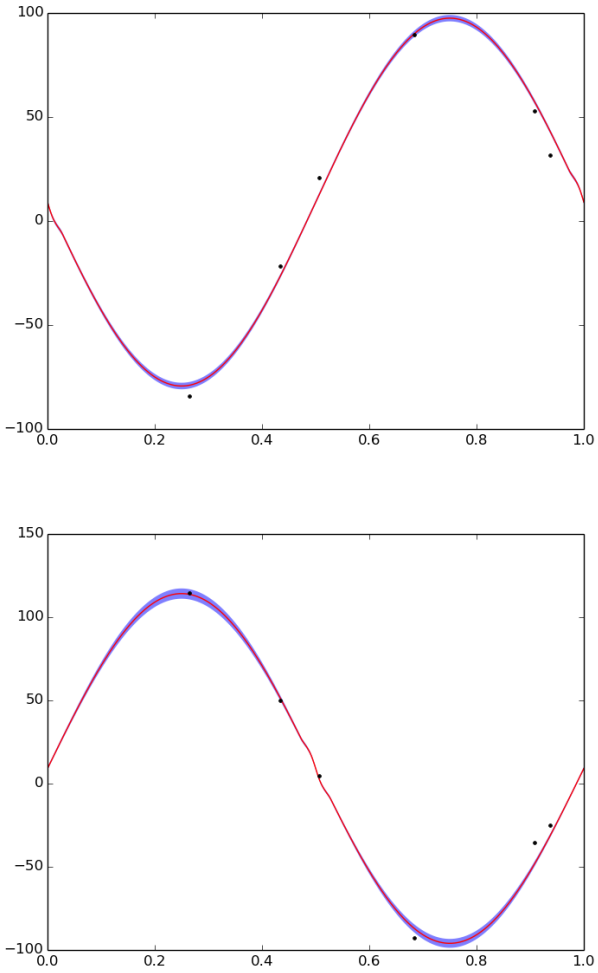

Figure 15: The individual RV data points and models from our analysis of the primary star (Top) and secondary star (Bottom). The black points are observational data while the red line is the best fit from our model. The blue are additional regions where parameters fit, but not the best fit.

Continuing to add the small set of known, bright M-M Dwarf eclipsing binary systems is of great importance to the stellar astronomy community. Creating a set of M Dwarf stars with model independent values for basic stellar parameters like Mass and Radius will be vital to furthering our understanding of these stars and answering questions like why our models consistently under predict parameters. We have outlined a successful procedure for finding these rare systems in large data sets of years long surveys and we hope others will follow our lead to continue to search for M-M Dwarf EBs.

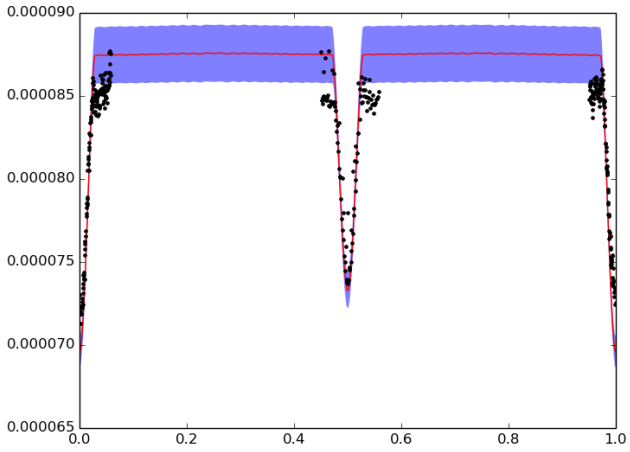

Figure 16: Our model fit to the Johnson I band follow-up observations. The black points are observational data and the red line is the best fit from the model. The blue are additional regions where parameters fit, but not the best fit.

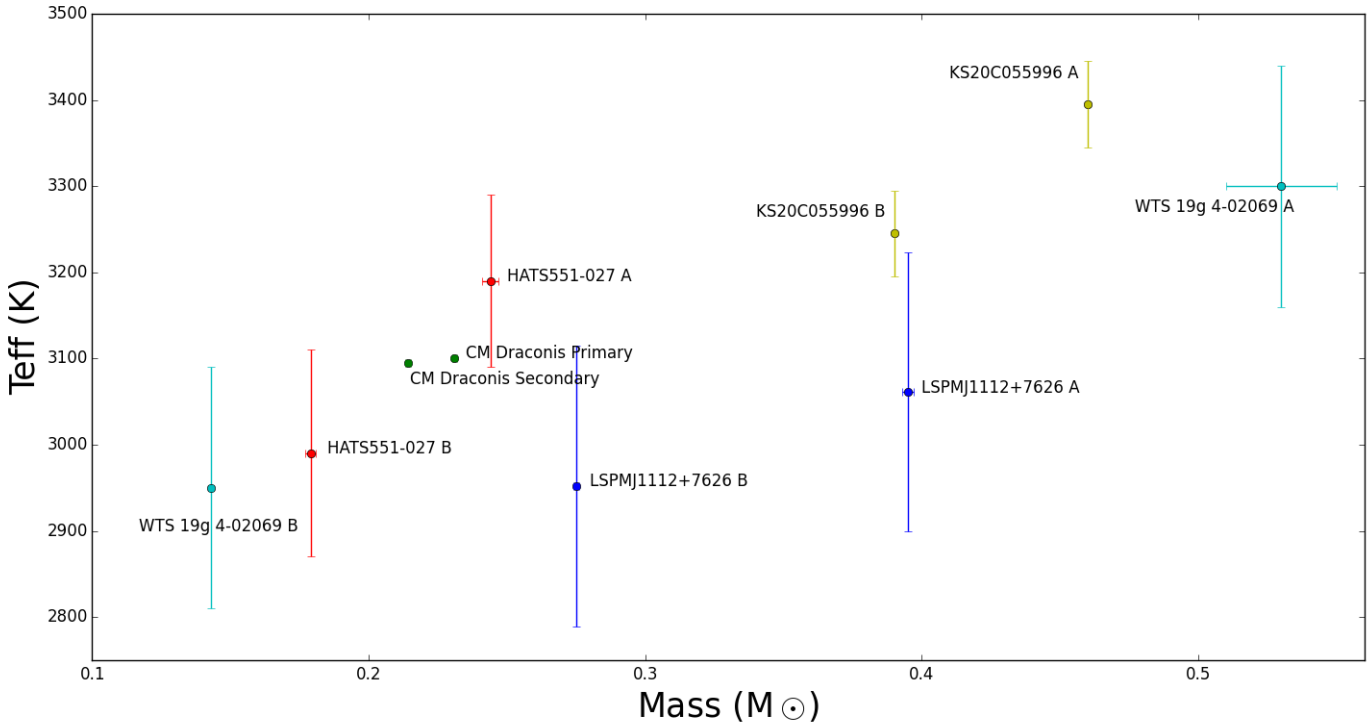

Figure 17: An update of Figure 1, we now show KS20C055996 in relation to previously known bright M-M Dwarf EBs.

References

F. Allard, D. Homeier, B. Freytag, and C. M. Sharp. Atmospheres From Very Low-Mass Stars to Extrasolar Planets. In C. Reylé, C. Charbonnel, and M. Schultheis, editors, *EAS Publications Series*, volume 57 of *EAS Publications Series*, pages 3–43, November 2012. doi: 10.1051/eas/1257001.

M. Asplund, N. Grevesse, A. J. Sauval, and P. Scott. The Chemical Composition of the Sun. *Annual Review of Astronomy and Astrophysics*, 47:481–522, September 2009. doi: 10.1146/annurev.astro.46.060407.145222.

I. Baraffe, G. Chabrier, F. Allard, and P. H. Hauschildt. Evolutionary models for solar metallicity low-mass stars: mass-magnitude relationships and color-magnitude diagrams. *Astronomy and Astrophysics*, 337:403–412, September 1998.

M. S. Bessell. Spectrophotometry: Revised Standards and Techniques. *Publications of the Astronomical Society of the Pacific*, 111:1426–1433, November 1999. doi: 10.1086/316454.

T. S. Boyajian, K. von Braun, G. van Belle, H. A. McAlister, T. A. ten Brummelaar, S. R. Kane, P. S. Muirhead, J. Jones, R. White, G. Schaefer, D. Ciardi, T. Henry, M. López-Morales, S. Ridgway, D. Gies, W.-C. Jao, B. Rojas-Ayala, J. R. Parks, L. Sturmann, J. Sturmann, N. H. Turner, C. Farrington, P. J. Goldfinger, and D. H. Berger. Stellar Diameters and Temperatures. II. Main-sequence K- and M-stars. *The The Astrophysical Journal*, 757:112, October 2012. doi: 10.1088/0004-637X/757/2/112.

D. Burger, K. G. Stassun, J. Pepper, R. J. Siverd, M. Paegert, N. M. De Lee, and W. H. Robinson. Filtergraph: An interactive web application for visualization of astronomy datasets. *Astronomy and Computing*, 2:40–45, August 2013. doi: 10.1016/j.ascom.2013.06.002.

G. Chabrier and I. Baraffe. Theory of Low-Mass Stars and Substellar Objects. *Annual Review of Astronomy and Astrophysics*, 38:337–377, 2000. doi: 10.1146/annurev.astro.38.1.337.

A. Collier Cameron, D. M. Wilson, R. G. West, L. Hebb, X.-B. Wang, S. Aigrain, F. Bouchy, D. J. Christian, W. I. Clarkson, B. Enoch, M. Esposito, E. Guenther, C. A. Haswell, G. Hébrard, C. Hellier, K. Horne, J. Irwin, S. R. Kane, B. Loeillet, T. A. Lister, P. Maxted, M. Mayor, C. Moutou, N. Parley, D. Pollacco, F. Pont, D. Queloz, R. Ryans, I. Skillen, R. A. Street, S. Udry, and P. J. Wheatley. Efficient identification of exoplanetary transit candidates from SuperWASP light curves. *Monthly Notices of the Royal Astronomical Society*, 380:1230–1244, September 2007. doi: 10.1111/j.1365-2966.2007.12195.x.

R. M. Cutri, M. F. Skrutskie, S. van Dyk, C. A. Beichman, J. M. Carpenter, T. Chester, L. Cambresy, T. Evans, J. Fowler, J. Gizis, E. Howard, J. Huchra, T. Jarrett, E. L. Kopan, J. D. Kirkpatrick, R. M. Light, K. A. Marsh, H. McCallon, S. Schneider, R. Stiening, M. Sykes, M. Weinberg, W. A. Wheaton, S. Wheelock, and N. Zacarias. VizieR Online Data Catalog: 2MASS All-Sky Catalog of Point Sources (Cutri+ 2003). *VizieR Online Data Catalog*, 2246:0, June 2003.

R. M. Cutri, E. L. Wright, Conrow T., and at al. VizieR Online Data Catalog: WISE All-Sky Data Release (Cutri+ 2012). *VizieR Online Data Catalog*, 2311:0, 2012.

A. Dotter, B. Chaboyer, D. Jevremović, V. Kostov, E. Baron, and J. W. Ferguson. The Dartmouth Stellar Evolution Database. *The Astrophysical Journal, Supplement*, 178:89–101, September 2008. doi: 10.1086/589654.

D. Foreman-Mackey, D. W. Hogg, D. Lang, and J. Goodman. emcee: The MCMC Hammer. *Publications of the Astronomical Society of the Pacific*, 125:306–312, March 2013. doi: 10.1086/670067.

M. Hamuy, A. R. Walker, N. B. Suntzeff, P. Gigoux, S. R. Heathcote, and M. M. Phillips. Southern spectrophotometric standards. *Publications of the Astronomical Society of the Pacific*, 104:533–552, July 1992. doi: 10.1086/133028.

J. Hartman. VARTOOLS: Light Curve Analysis Program. Astrophysics Source Code Library, August 2012.

G. Kovács, S. Zucker, and T. Mazeh. A box-fitting algorithm in the search for periodic transits. *Astronomy and Astrophysics*, 391:369–377, August 2002. doi: 10.1051/0004-6361:20020802.

G. Kovács, G. Bakos, and R. W. Noyes. A trend filtering algorithm for wide-field variability surveys. *Monthly Notices of the Royal Astronomical Society*, 356: 557–567, January 2005. doi: 10.1111/j.1365-2966.2004.08479.x.

C. J. Lada. Stellar Multiplicity and the Initial Mass Function: Most Stars Are Single. *The Astrophysical Journal, Letters*, 640:L63–L66, March 2006. doi: 10.1086/503158.

S. Lépine, E. J. Hilton, A. W. Mann, M. Wilde, B. Rojas-Ayala, K. L. Cruz, and E. Gaidos. A Spectroscopic Catalog of the Brightest (J 9) M Dwarfs in the Northern Sky. *The Astronomical Journal*, 145:102, April 2013. doi: 10.1088/0004-6256/145/4/102.

M. López-Morales. On the Correlation between the Magnetic Activity Levels, Metallicities, and Radii of Low-Mass Stars. *The Astrophysical Journal*, 660: 732–739, May 2007. doi: 10.1086/513142.

M. López-Morales and I. Ribas. GU Bootis: A New 0.6 M_{solar} Detached Eclipsing Binary. *The Astrophysical Journal*, 631:1120–1133, October 2005. doi: 10.1086/432680.

J. C. Morales, I. Ribas, C. Jordi, G. Torres, J. Gallardo, E. F. Guinan, D. Charbonneau, M. Wolf, D. W. Latham, G. Anglada-Escudé, D. H. Bradstreet, M. E. Everett, F. T. O'Donovan, G. Mandushev, and R. D. Mathieu. Absolute Properties of the Low-Mass Eclipsing Binary CM Draconis. *The Astrophysical Journal*, 691:1400–1411, February 2009. doi: 10.1088/0004-637X/691/2/1400.

J. Pepper and K. Stassun. Target Selection for the TESS Mission. In *AAS/Division for Extreme Solar Systems Abstracts*, volume 3 of *AAS/Division for Extreme Solar Systems Abstracts*, page 114.11, December 2015.

J. Pepper, R. W. Pogge, D. L. DePoy, J. L. Marshall, K. Z. Stanek, A. M. Stutz, S. Poindexter, R. Siverd, T. P. O'Brien, M. Trueblood, and P. Trueblood. The Kilodegree Extremely Little Telescope (KELT): A Small Robotic Telescope for Large-Area Synoptic Surveys. *Publications of the Astronomical Society of the Pacific*, 119:923–935, August 2007. doi: 10.1086/521836.

J. Pepper, R. B. Kuhn, R. Siverd, D. James, and K. Stassun. The KELT-South Telescope. *Publications of the Astronomical Society of the Pacific*, 124:230–241, March 2012. doi: 10.1086/665044.

D. Reichart, M. Nysewander, J. Moran, J. Bartelme, M. Bayliss, A. Foster, J. C. Clemens, P. Price, C. Evans, J. Salmonson, S. Trammell, B. Carney, J. Keohane, and R. Gotwals. PROMPT: Panchromatic Robotic Optical Monitoring and Polarimetry Telescopes. *Nuovo Cimento C Geophysics Space Physics C*, 28:767, July 2005. doi: 10.1393/ncc/i2005-10149-6.

I. N. Reid, S. L. Hawley, and J. E. Gizis. The Palomar/MSU Nearby-Star Spectroscopic Survey. I. The Northern M Dwarfs -Bandstrengths and Kinematics. *The Astronomical Journal*, 110:1838, October 1995. doi: 10.1086/117655.

I. Ribas. Masses and Radii of Low-Mass Stars: Theory Versus Observations. *Astrophysics and Space Science*, 304:89–92, August 2006. doi: 10.1007/s10509-006-9081-4.

G. R. Ricker, J. N. Winn, R. Vanderspek, D. W. Latham, G. Á. Bakos, J. L. Bean, Z. K. Berta-Thompson, T. M. Brown, L. Buchhave, N. R. Butler, R. P. Butler, W. J. Chaplin, D. Charbonneau, J. Christensen-Dalsgaard, M. Clampin, D. Deming, J. Doty, N. De Lee, C. Dressing, E. W. Dunham, M. Endl, F. Fressin, J. Ge, T. Henning, M. J. Holman, A. W. Howard, S. Ida, J. M. Jenkins, G. Jernigan, J. A. Johnson, L. Kaltenegger, N. Kawai, H. Kjeldsen, G. Laughlin, A. M. Levine,

D. Lin, J. J. Lissauer, P. MacQueen, G. Marcy, P. R. McCullough, T. D. Morton, N. Narita, M. Paegert, E. Palle, F. Pepe, J. Pepper, A. Quirrenbach, S. A. Rinehart, D. Sasselov, B. Sato, S. Seager, A. Sozzetti, K. G. Stassun, P. Sullivan, A. Szentgyorgyi, G. Torres, S. Udry, and J. Villasenor. Transiting Exoplanet Survey Satellite (TESS). *Journal of Astronomical Telescopes, Instruments, and Systems*, 1(1):014003, January 2015. doi: 10.1117/1.JATIS.1.1.014003.

D. Ségransan, P. Kervella, T. Forveille, and D. Queloz. First radius measurements of very low mass stars with the VLTI. *Astronomy and Astrophysics*, 397:L5–L8, January 2003. doi: 10.1051/0004-6361:20021714.

M. F. Skrutskie, R. M. Cutri, R. Stiening, M. D. Weinberg, S. Schneider, J. M. Carpenter, C. Beichman, R. Capps, T. Chester, J. Elias, J. Huchra, J. Liebert, C. Lonsdale, D. G. Monet, S. Price, P. Seitzer, T. Jarrett, J. D. Kirkpatrick, J. E. Gizis, E. Howard, T. Evans, J. Fowler, L. Fullmer, R. Hurt, R. Light, E. L. Kopan, K. A. Marsh, H. L. McCallon, R. Tam, S. Van Dyk, and S. Wheelock. The Two Micron All Sky Survey (2MASS). *The Astronomical Journal*, 131:1163–1183, February 2006. doi: 10.1086/498708.

R. C. Terrien, S. Mahadevan, C. F. Bender, R. Deshpande, and P. Robertson. M Dwarf Luminosity, Radius, and α-enrichment from I-band Spectral Features. *Astrophysical Journal, Letters*, 802:L10, March 2015. doi: 10.1088/2041-8205/802/1/L10.

N. Zacharias, C. T. Finch, T. M. Girard, A. Henden, J. L. Bartlett, D. G. Monet, and M. I. Zacharias. VizieR Online Data Catalog: UCAC4 Catalogue (Zacharias+, 2012). *VizieR Online Data Catalog*, 1322, July 2012.

N. Zacharias, C. T. Finch, T. M. Girard, A. Henden, J. L. Bartlett, D. G. Monet, and M. I. Zacharias. The Fourth US Naval Observatory CCD Astrograph Catalog (UCAC4). *The Astronomical Journal*, 145:44, February 2013. doi: 10.1088/0004-6256/145/2/44.

G. Zhou, D. Bayliss, J. D. Hartman, M. Rabus, G. Á. Bakos, A. Jordán, R. Brahm, K. Penev, Z. Csubry, L. Mancini, N. Espinoza, M. de Val-Borro, W. Bhatti, S. Ciceri, T. Henning, B. Schmidt, S. J. Murphy, R. P. Butler, P. Arriagada, S. Shectman, J. Crane, I. Thompson, V. Suc, and R. W. Noyes. A 0.24+0.18 M double-lined eclipsing binary from the HATSouth survey. *Monthly Notices of the Royal Astronomical Society*, 451:2263–2277, August 2015. doi: 10.1093/mnras/stv1070.